Nonlinear ultrasonic response of voids and Cu precipitates in body-centered cubic Fe

Wahyu Setyawan,[a] Charles H. Henager, Jr., and Shenyang Hu[b]

Pacific Northwest National Laboratory, Richland, Washington 99352, USA

Interpreting nonlinear ultrasonic signals detected in a nondestructive evaluation of radiation damage requires the knowledge of the correlation between defects and nonlinearity. In this work, molecular dynamics simulations are performed to study the effect of distributed vacancies, voids, Cu atoms, and Cu precipitates on the nonlinear ultrasonic response in body-centered cubic (bcc) Fe. The nonlinearity parameter calculated from the second harmonic amplitude in the perfect lattice is 2.73. Vacancies are found to increase the nonlinearity. However, clusters of vacancies in the form of spherical voids show an opposite effect. This finding can be used to conveniently distinguish vacancies from voids in the material. Unlike vacancies, individual Cu atoms decrease the nonlinearity. Clustering of Cu atoms into Cu precipitates further decreases the nonlinearity. Interestingly, precipitates with a diameter of 2 nm and larger exhibit a similar effect despite their different structure and coherency with the Fe matrix. *Published by AIP Publishing.*
https://doi.org/10.1063/1.5029368

I. INTRODUCTION

Anharmonic terms of potential energy of atoms in a real crystal bring about interesting phenomena.[1,2] A visible anharmonic effect is the thermal expansion of the crystal. Another direct manifestation is that the elasticity, i.e., the stress-strain relationship, of the crystal is nonlinear. In such a medium, if one transmits a sinusoidal acoustic wave with a fundamental frequency f, higher order harmonic waves will be generated as the original wave travels through the crystal. Defects present in a real solid inevitably modify the potential energy landscape, hence the propensity of the solid to generate the harmonics. Therefore, by carefully examining the change in the amplitude of the harmonics, one can reveal the presence of the defects. An excellent review on this topic can be found in Ref. 3.

High-energy particle irradiation (such as neutrons, ions, and electrons) continuously generates defects such as vacancies, interstitials, and their clusters in nuclear fuels and structural components of nuclear reactors.[4,5] The radiation defects accelerate microstructure evolution, hence thermomechanical property degradation of materials.[6–9] Therefore, monitoring defect and microstructure evolution and thermomechanical property degradation in nuclear materials is crucial for the life extension of current reactor fleets and advanced reactor designs. Nonlinear ultrasonic (NLUS) measurements are based on the fact that as a sinusoidal wave propagates through a nonlinear medium, a second harmonic (SH) wave is generated. The measured response is usually quantified in terms of the acoustic nonlinearity parameter.[10–13] Experiments[14–17] demonstrated the sensitivity of NLUS to irradiation-induced defects in a reactor pressure vessel (RPV) steel and suggested that material degradation

could be followed using the nonlinearity parameter. However, the microstructure in irradiated materials is complicated. Different defects such as vacancies, interstitials, vacancy clusters, interstitial loops, second phase precipitates, and dislocations might coexist. While in theory detecting the harmonics to deduce various types of defect is plausible, it is often challenging to diagnose different types of defects experimentally and to determine which ones are of importance to assess the thermo-mechanical properties. In this respect, simulations are well-suited to decipher the contribution of each defect species.

In this paper, we apply the principle of second harmonic generation to study the correlation between defects and the nonlinearity parameter in body-centered cubic (bcc) Fe. The defects include individual vacancies, voids, individual Cu atoms, and Cu precipitates. Studying these defects in the Fe matrix is particularly relevant for modeling neutron-irradiated reactor pressure vessel steels. The main objective is to investigate the sensitivity of SH generation due to each of these defects and to develop the correlations between defects and the nonlinearity parameter for decoding nonlinear ultrasonic signals detected in nondestructive evaluation of radiation damage.

II. METHOD

Molecular dynamics (MD) simulation is employed with an empirical interatomic potential to study the nonlinear effects. The simulations are performed using the LAMMPS code[18] with Fe-Cu interatomic potential from Ref. 19 in which the Fe interaction was from Ref. 20 and the Cu interaction was from Ref. 21. The potential has been shown to reproduce well the experimental thermodynamic properties of the Fe-Cu alloy and *ab initio* interaction energies between Cu atoms and point defects in Fe. High-resolution electron microscopy experiments have revealed that a Cu precipitate

---

[a] Electronic mail: wahyu.setyawan@pnnl.gov
[b] Electronic mail: shenyang.hu@pnnl.gov

in bcc Fe undergoes a bcc $\rightarrow$ 9R transformation when the diameter of the precipitate is larger than a critical size.[22,23] This critical size depends on temperature, e.g., about 9 nm at 400 °C and 4 nm at –6 °C. We have validated the potential by looking at the structure of the Cu precipitate at zero K, in which we found that a 2-nm precipitate indeed remains bcc (coherent with the Fe matrix), while a 7-nm precipitate undergoes the above transformation.

All simulations to study the nonlinear effects are performed at zero K. The simulation box is constructed with the x, y, and z axes oriented along the [100], [010], and [001] crystal directions of the bcc Fe, respectively. Periodic boundaries are applied only along y and z to render the crystal infinite along these directions. The ultrasonic wave will be propagated along the $+x$ direction. Several regions of atoms are defined along x. A source region is located at the front end ($x = 0$), a detector region is located at $x = x_D$, and a backend region is located at the back end. Each region consists of two layers of atoms.

Since both ends of the x dimension represent free surfaces, it is necessary to initially relax the atoms to their equilibrium positions before being subjected to an ultrasonic wave. A few layers of the surface atoms recede inwards upon minimization. After this minimization, the positions of atoms in the backend region are fixed. A longitudinal elastic wave is introduced by periodically displacing atoms in the source region along x according to a given frequency (f). In other words, the position of these atoms is not obtained from the time-integration of their equation of motion due to the forces they experience (forces acting on atoms at the source region that are not used to update their position), but rather the position is updated every timestep such that their position is given by $x = x_0 + a_{1s}\sin(2\pi ft)$ where x_0 is the initial position and a_{1s} is the amplitude of the displacement. As a result, a longitudinal pressure wave is experienced by subsequent atoms behind the source region and the pressure wave is propagated. The choice of the amplitude and period of the sine wave will be discussed later. The x-displacement of atoms in the detector region, averaged over atoms in this

region, is recorded as a function of time and is taken as the detector signal. The detector signal is collected up until before the reflected wave off the backend reaches the detector.

Figure 1(a) shows a schematic of the simulation setup. The longitudinal sound wave is propagated along the x direction as shown with the arrow. In this setup, the period of the wave is $T = 2$ ps, i.e., its frequency is $f = 0.5$ THz. The snapshot is taken after approximately four complete cycles have been excited at the source. The red and blue regions represent atoms in a positive and negative x-displacement, respectively. The source is turned off after four cycles. Figure 1(b) shows the time evolution of the signal at the source and at a detector located 570 Å away. In this setup, the total length of the x dimension is $304a \approx 868$ Å (where a is the bcc lattice constant of 2.8553 Å). The initial rise of the detector signal is non-sinusoidal because of atom's inertia. Accordingly, a three-cycle signal (a portion of the signal spanning a duration of $3T$) is taken after the first + to – sign change for fast Fourier transform (FFT) analysis. This $3T$ portion of the signal is plotted as a black curve and labelled "FFT duration" as shown in Fig. 1(b). The sampling rate of the FFT is $N_s = 200$ data points per cycle. To calculate the FFT, let $x[n] = [x_0, x_1, \ldots, x_{N-1}]$ be the sequence of the sampled data points from MD. N is the total number of samples, $N = N_c N_s$, where N_c is the number of cycles of the signal duration taken for FFT, in this case $N_c = 3$. The FFT of $x[n]$ results in another sequence of numbers $X[p] = [X_0, X_1, \ldots, X_{N-1}]$ where the X_p component is given by

$$X_p = \sum_{n=0}^{N-1} x_n e^{-i2\pi pn/N}, \tag{1}$$

where i is the imaginary number. The frequency associated with the FFT component X_p is simply $f_p = p/(N_c T)$. Therefore, $p = N_c, 2N_c, 3N_c$, and so on corresponds to the fundamental component, second harmonic, third harmonic, and so on. An FFT amplitude spectrum is a plot of the magnitude of X_p as a function of p, i.e., $|X_p|$ vs p or equivalently $|X_p|$ vs f_p. Figure 1(c) shows the FFT amplitude spectrum of
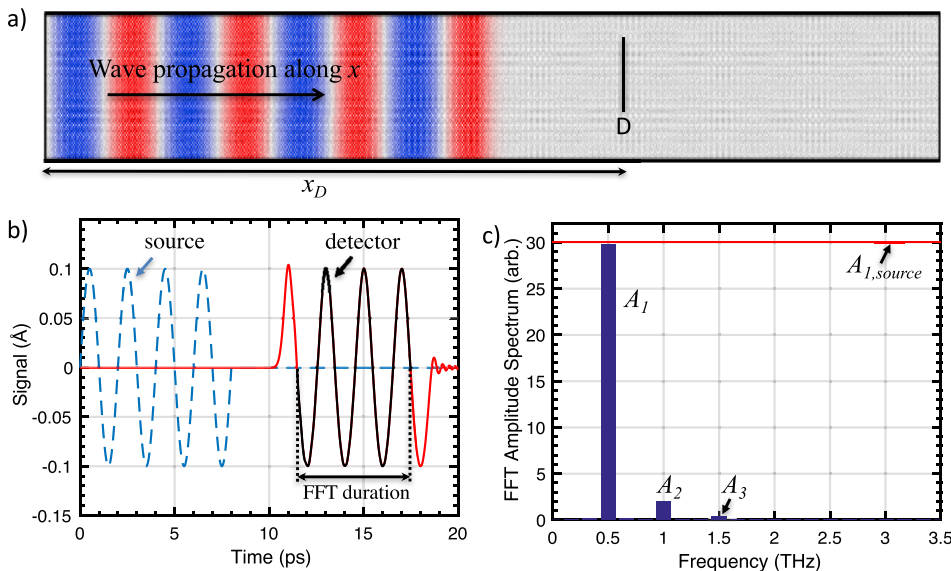

FIG. 1. (a) A snapshot of the pressure wave (period $T = 2$ ps) propagating along x in bcc Fe. Atoms are colored according to their x-displacement showing a positive (red) or a negative (blue) displacement. A detector D is set up to monitor the displacement field. (b) Time evolution of the signal received at a detector at $x_D = 570$ Å, and the length of the box along x is $\sim$868 Å. A three-cycle portion of the detector signal labelled as "FFT duration" is taken for FFT. (c) FFT amplitude spectrum of the detector revealing the second (A_2) and third (A_3) harmonic generation.

the detector, revealing the generation of the second and third harmonics at 1 and 1.5 THz, respectively. In Fig. 1(c), the FFT amplitude of the fundamental wave, second, and third harmonics is denoted as A_1, A_2, and A_3, respectively. The original sequence $x[n]$ can be recovered from the inverse FFT of $X[p]$, where the x_n sample is given by

$$x_n = \frac{1}{N}\sum_{p=0}^{N-1} X_p e^{i2\pi pn/N}. \tag{2}$$

For a real-valued signal such as in our case (i.e., $x[n]$ is a series of real numbers), the relationship $X_{N-p} = X_p^*$ is valid (where X_p^* is the complex conjugate of X_p).

As an example, suppose the detector signal $x[n] = u_1[n] + u_2[n]$ is composed of a fundamental signal $u_1[n] = a_1\sin(2\pi N_c n/N)$ and a second harmonic signal $u_2[n] = a_2\sin(2\pi(2N_c)n/N)$. By employing the relation of $\sin(y) = (e^{iy} - e^{-iy})/2i$, all X_p is zero except for $p = N_c$, $N - N_c$, $2N_c$, and $N - 2N_c$

$$\begin{aligned} X_{p=N_c} &= Na_1/(2i), \\ X_{p=N-N_c} &= -Na_1/(2i), \\ X_{p=2N_c} &= Na_2/(2i), \\ X_{p=N-2N_c} &= -Na_2/(2i), \end{aligned} \tag{3}$$

where in this case, the FFT amplitude A_1 is $= Na_1/2$ and FFT amplitude A_2 is $= Na_2/2$. Therefore, knowing A_1 and A_2, the amplitude of the fundamental signal (a_1) and the second harmonic a_2 can be determined. The value of a_2 will be needed when we calculate the nonlinearity parameter β.

III. RESULTS AND DISCUSSION

With the above setup, we analyze the generation as a function of distance for two different fundamental frequencies, $f = 0.5$ and 1 THz, as shown in Fig. 2. These high frequencies are employed in MD because the practical length scale is typically limited to $\sim 1\,\mu m$. The longitudinal speed of sound along [100] calculated from MD is 5393 m/s, in close agreement with the experimental value of 5130 m/s. Given the above speed of sound, a frequency of 0.5 THz corresponds to a wavelength of $\lambda = 107.85\,\text{Å} \approx 38a$ and the x dimension of the box is approximately equal to 8λ. With the 0.5 THz excitation, the fundamental amplitude decreases almost unnoticeably in Fig. 2, while the fundamental signal from the 1 THz source decreases considerably. The second harmonic from the 0.5 THz source increases linearly with the distance, while that from the 1 THz does not. As the original wave travels through the crystal, a portion of the elastic energy is transformed to generate its harmonics with frequency $2f$, $3f$, $4f$, and so forth. Similarly, as the second harmonic is generated, a portion of its energy is transformed to generate its harmonics, in this case with frequency $4f$, $6f$, $8f$, and so forth. The linear behavior of the second harmonic from the 0.5 THz source indicates that very little energy is converted to the higher harmonics. In other words, the amplitude of the second harmonic is proportional to the number of nonlinearity-generating centers, in this case atoms; therefore,
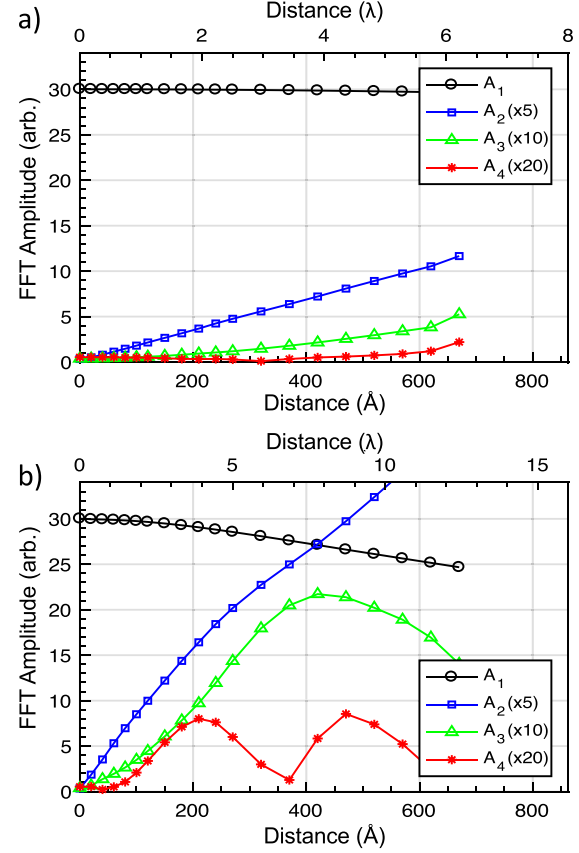

FIG. 2. Decay of the fundamental signal (A_1) and generation of the second (A_2), third (A_3), and fourth (A_4) harmonics as a function of distance for an excitation frequency of (a) 0.5 THz and (b) 1 THz. The curves for A_2, A_3, and A_4 have been multiplied by 5, 10, and 20 for clarity, respectively.

it accumulates linearly with distance. This is not the case with the 1 THz source as can be seen from the considerable amplitude of the third and fourth harmonics in Fig. 2(b). From this observation, we set the frequency of the excitation at 0.5 THz. The amplitude of the excitation is kept at 0.1 Å since it yields reliable harmonics.

For the rest of the simulations, the x dimension of $304a$ ($\sim 8\lambda$) is used with the detector placed at $x_D = 5\lambda$. This setup allows for the four cycles of the wave to pass through the detector before the reflected wave reaches the detector. The y and z dimensions are chosen depending on the size and concentration of the defect that is studied.

Consider a nonlinearly elastic medium in which only the leading nonlinear term is kept in the stress-strain relationship $\sigma(\epsilon)$

$$\sigma = A\epsilon + \frac{1}{2}B\epsilon^2, \tag{4}$$

where the strain is simply the gradient of the displacement $\epsilon = \partial u/\partial x$. The ratio B/A is known as the nonlinearity parameter β. The solution of a one-dimensional pressure wave equation for a given excitation of the form $u = a_{1s}\sin(\omega t)$ is presented in Ref. 11 with the second harmonic term given by

$$u_2 = \frac{B}{8A}(a_{1s}k)^2 x\,\cos[2(kx - \omega t)], \tag{5}$$

where k is the wave number. From Eq. (5), the amplitude of the second harmonic a_2 increases linearly with distance. This

behavior is exhibited by the 0.5 THz excitation with $a_{1s} = 0.1$ Å as previously shown in Fig. 2. Equivalently, knowing the second harmonic amplitude, the nonlinearity parameter can be calculated from

$$\beta = \frac{8a_2}{x(a_{1s}k)^2}. \tag{6}$$

For a perfect bcc Fe, the intrinsic nonlinearity parameter for a longitudinal sound wave propagating along the [100] crystal direction is calculated to be $\beta_0 = 2.73$.

Subsequently, we study how the nonlinearity parameter changes with the presence of distributed mono vacancies, simply referred to as vacancies. The vacancies are randomly distributed in the region between the source and the detector. It is found that vacancies increase the anharmonic effect. The ratio of the nonlinearity parameter relative to the intrinsic value, β/β_0, is plotted in Fig. 3 as a function of concentration. The ratio increases linearly with a slope of $\sim 0.15/(1\%)$ = 15 (note that the concentration in Fig. 3 is given in percentage).

For a given vacancy concentration, the effect of clustering is studied by simulating spherical voids. Two void sizes, 2 and 7 nm in diameter, are investigated. To appreciate the scale of the simulation, to study a 7-nm void containing an equivalent vacancy concentration (point-defect-equivalent) of 0.1%, a simulation box of $304 \times 200 \times 200$ supercells containing more than 24×10^6 atoms is needed. Voids are placed randomly, except for concentrations that correspond to only one void, in which case it is placed midway between the source and the detector. The nonlinearity ratios obtained with the 2-nm and 7-nm voids are plotted in Fig. 3 as a function of point-defect-equivalent concentration, together with the curve for vacancies for comparison. While vacancies increase the anharmonic effect, voids suppress it. This finding suggests that vacancies can be readily distinguished from voids. The linear fits of the 2-nm and 7-nm curves are practically the same, indicating that voids of size 2 nm and larger induce a similar anharmonic effect. The slope of the fits for
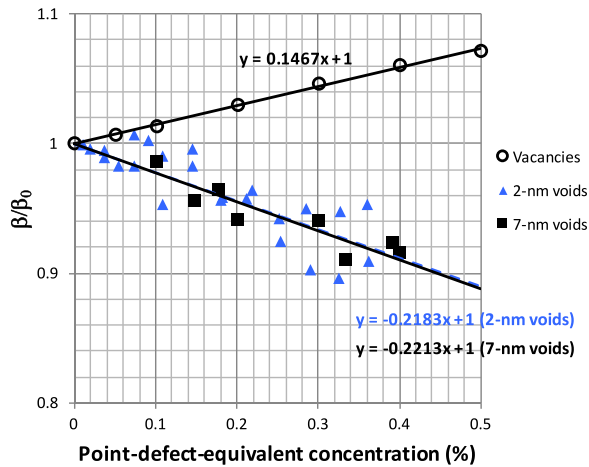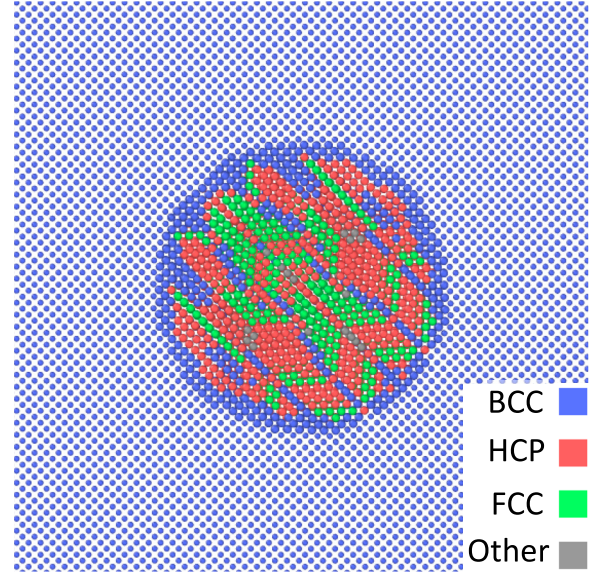

FIG. 4. 1-nm thick cross-section cut on the yz-plane through a 7-nm Cu precipitate in the bcc Fe matrix after structure relaxation. Atoms are colored based on a Common Neighbor Analysis revealing that the precipitate has transformed from bcc to an incoherent 9R type of a structure consisting of rotated segments of hcp and fcc structures.

voids is $-0.22/(1\%) = -22$. We note that the linear relationships provide a convenient way to interpolate towards a lower concentration regime that is computationally impractical to model.

Spherical Cu precipitates are studied with the same setup as the voids. Initially, Cu precipitates are created in a bcc phase coherent with the Fe matrix. Upon the initial relaxation, a 2-nm precipitate remains in bcc, while a 7-nm precipitate transforms to a structure as shown in Fig. 4. A common neighbor analysis reveals that the larger precipitate has transformed into a structure consisting of a mixture of mostly hexagonal close-packed (hcp) and face-centered cubic (fcc) arrangements. The herringbone patterns within the hcp and fcc regions are reminiscent of the 9R structure.[22] In addition to Cu precipitates, the effect of distributed Cu

FIG. 3. Ratio of nonlinearity parameter, β/β_0, due to vacancies, 2-nm and 7-nm diameter voids, relative to the perfect crystal, as a function of point-defect-equivalent concentration. The period of the fundamental wave is period $T = 2$ ps.
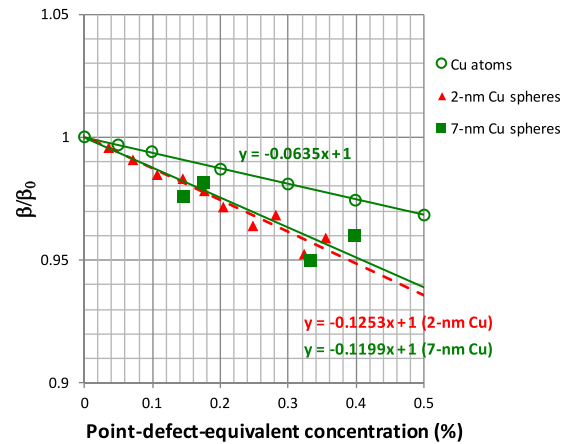

FIG. 5. Ratio of nonlinearity parameter, β/β_0, due to individual Cu atoms, 2-nm, and 7-nm diameter Cu precipitates, relative to the perfect crystal, as a function of point-defect-equivalent concentration. The period of the fundamental wave is period $T = 2$ ps.
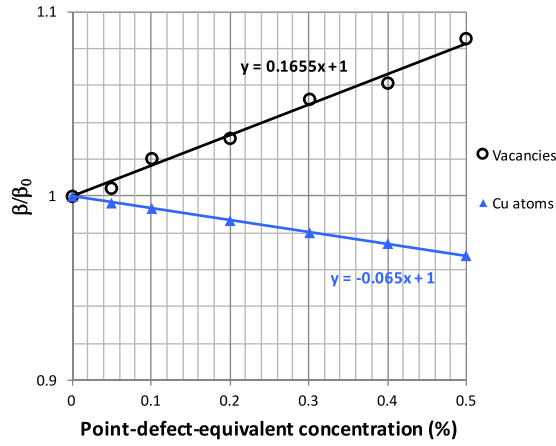
FIG. 6. Ratio of nonlinearity parameter, β/β_0, due to vacancies and individual Cu atoms, relative to the perfect crystal, as a function of point-defect-equivalent concentration. The period of the fundamental wave is period $T = 4$ ps.

atoms is also studied. Figure 5 shows the ratio of the nonlinearity parameter as a function of concentration obtained with the Cu atoms and Cu precipitates. The results show that Cu atoms and Cu precipitates decrease the anharmonic effect. The linear fits show that 2-nm Cu precipitates influence the nonlinearity roughly twice as strongly as individual Cu atoms. Interestingly, the effect of 2-nm Cu is practically the same as that of 7-nm Cu, suggesting that the structure and/or coherency of the Cu precipitates have a negligible effect on the nonlinearity.

A bench mark study is performed to investigate the effect of frequency. The results presented so far are obtained with a fundamental wave with $T = 2$ ps. A longer wave, $T = 4$ ps, is used for the bench mark study. Simple systems (vacancies and Cu atoms) are tested. The ratio of the nonlinearity parameter is shown in Fig. 6. For vacancies, the slope is $0.166/(1\%) = 16.6$ ($T = 4$ ps) compared to 14.7 ($T = 2$ ps). For Cu atoms, the slope is $-0.065/(1\%) = -6.5$ ($T = 4$ ps) compared to -6.4 ($T = 2$ ps). The differences are very small. As previously shown in Fig. 2, the second harmonic

generation is linear with distance for a fundamental wave with $T = 2$ ps but is not the case for $T = 1$ ps because for $T = 1$ ps or lower, third and higher harmonics start to play a role (i.e., the second harmonic starts to lose its energy and converted to higher harmonics; hence, it is no longer linear with the distance). Hence, the results from the bench mark study further indicate that the results presented in this work are also valid for ultrasonic waves with a longer period as long as the generation of the third and higher harmonics can be considered negligible (i.e., as long as Eq. (5) is satisfied). Equation (5) can also be achieved in practice even though a much lower frequency (e.g., 10 MHz) is employed in experiments[11] compared to 500 and 250 GHz in the MD simulations. Note that Eq. (5) also implies that the amplitude of the second harmonic is proportional to the square of the fundamental wave amplitude. In experiments, this relationship can be more readily measured to examine whether Eq. (5) is satisfied by varying the voltage of the wave generator compared to the linear increase in the second harmonic with the distance where specimens with varying thickness would be needed. Experiments on Al single-crystal specimens with 10 MHz wave clearly showed the above relationship between the amplitudes of the second harmonic and the fundamental wave.[11] Therefore, the results presented in this MD study are expected to be applicable for 10 MHz waves, which are typically employed in experiments, provided that Eq. (5) is satisfied.

To gain insights into the origin of the behavior of β for vacancies and Cu atoms, tensile simulations are performed for systems with a point defect concentration of 0.3%. Figure 7 shows the plots of true stress vs true strain for the perfect system, systems with vacancies, and systems with Cu atoms. The plots are fitted using Eq. (4). The fitted values of the coefficients A and B are given in the figure. $\beta = B/A$ is then calculated. They are $\beta_0 = 2.77$ (perfect), $\beta = 2.87$ (vacancies), and $\beta = 2.72$ (Cu atoms). The elasticity simulations show that vacancies increase β, while Cu atoms decrease β compared to the perfect system, consistent with the ultrasonic simulations.
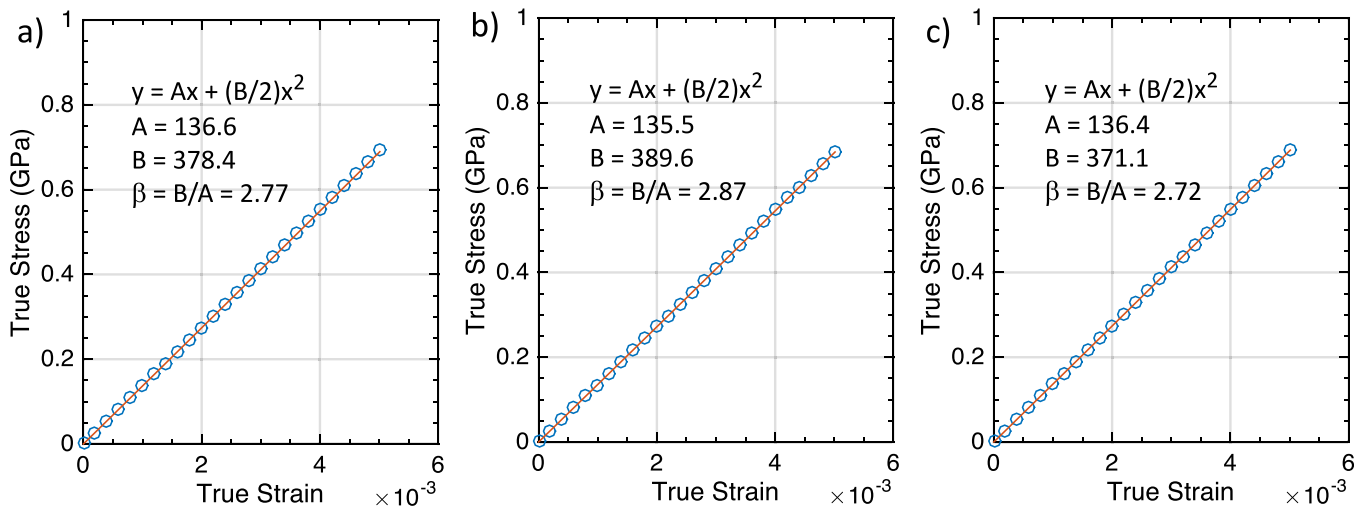

FIG. 7. Tensile simulation for (a) perfect crystal, (b) crystal with 0.3% vacancies, and (c) with 0.3% Cu atoms.

IV. CONCLUSION

In all cases, the change in the anharmonic effect is linear with concentration. A striking difference in the second harmonic response is discovered between vacancies and voids in bcc Fe. Vacancies increase the anharmonic effect relative to a perfect lattice, while voids decrease it. The opposite behavior allows vacancies to be readily distinguished from voids. Further simulations show that voids of diameter 2 nm and larger exhibit a similar effect and cannot be distinguished from one another. From the linear dependence of the nonlinearity parameter on the defect concentration, 1% volume swelling due to voids would reduce the nonlinearity parameter by more than 20%. Unlike vacancies, individual Cu atoms as well as Cu precipitates decrease the anharmonic effect. For a given point-defect-equivalent concentration, 2-nm diameter Cu precipitates change the anharmonic response twice as strongly as Cu atoms. For instance, the nonlinearity parameter reduces by 6% for a solid solution phase of Fe-1at.%Cu (1 atomic % of Cu), while Cu precipitates cause 12% reduction. Nevertheless, as in the case of voids, Cu precipitates of diameter 2 nm and 7 nm are not distinguishable even though the structure of the former remains coherent with the Fe matrix, while the latter transforms into an incoherent precipitate. Fundamental results in this study are useful for elucidating the anharmonic contribution of each defect species when different defect species are present, e.g., dislocations pinning by Cu precipitates, which will be explored in the future.

ACKNOWLEDGMENTS

[1]C. Kittel, *Introduction for Solid State Physics* (John Wiley & Sons, New York, 1996).

[2]M. Miniaci, A. S. Gliozzi, B. Morvan, A. Krushynska, F. Bosia, M. Scalerandi, and N. M. Pugno, "Proof of concept for an ultrasensitive technique to detect and localize sources of elastic nonlinearity using phononic crystals," Phys. Rev. Lett. **118**, 214301 (2017).

[3]K. H. Matlack, J. Y. Kim, L. J. Jacobs, and J. Qu, "Review of second harmonic generation measurement techniques for material state determination in metals," J. Nondestr. Eval. **34**, 273 (2014).

[4]D. J. Bacon, F. Gao, and Y. N. Osetsky, "The primary damage state in fcc, bcc and hcp metals as seen in molecular dynamics simulations," J. Nucl. Mater. **276**, 1–12 (2000).

[5]B. N. Singh and S. J. Zinkle, "Defect accumulation in pure fcc metals in the transient regime—A review," J. Nucl. Mater. **206**, 212–229 (1993).

[6]E. A. Little, "Microstructural evolution in irradiated ferritic-martensitic steels—Transitions to high-dose behavior," J. Nucl. Mater. **206**, 324–334 (1993).

[7]G. S. Was and S. M. Bruemmer, "Effects of irradiation on intergranular stress-corrosion cracking," J. Nucl. Mater. **216**, 326–347 (1994).

[8]S. J. Zinkle and B. N. Singh, "Microstructure of Cu-Ni alloys neutron irradiated at 210 °C and 420 °C to 14 DPa," J. Nucl. Mater. **283**, 306–312 (2000).

[9]F. A. Garner, M. B. Toloczko, and B. H. Sencer, "Comparison of swelling and irradiation creep behavior of fcc-austenitic and bcc-ferritic/martensitic alloys at high neutron exposure," J. Nucl. Mater. **276**, 123–142 (2000).

[10]J. Kyung-Young, "Applications of nonlinear ultrasonics to the nde of material degradation," IEEE Trans. Ultrason., Ferroelectr. Frequency Control **47**, 540–548 (2000).

[11]A. Hikata, B. B. Chick, and C. Elbaum, "Dislocation contribution to the second harmonic generation of ultrasonic waves," J. Appl. Phys. **36**, 229–236 (1965).

[12]K. Balasubramaniam, "Understanding of materials state and its degradation using nonlinear-ultrasound (nlu) approaches," Report No. aoard-094129 (Indian Institute of Technology Madras, 2011).

[13]G. E. Dace, R. B. Thompson, L. J. H. Brasche, D. K. Rehbein, and O. Buck, "Nonlinear acoustics, a technique to determine microstructural changes in materials," in *Review of Progress in Quantitative Nondestructive Evaluation: Volume 10B*, edited by D. O. Thompson and D. E. Chimenti (Springer US, Boston, MA, 1991), pp. 1685–1692.

[14]C. Kim and I. Park, "Microstructural degradation assessment in pressure vessel steel by harmonic generation technique," J. Nucl. Sci. Technol. **45**, 1036–1040 (2008).

[15]K. H. Matlack, J. Y. Kim, J. J. Wall, J. Qu, L. J. Jacobs, and M. A. Sokolov, "Sensitivity of ultrasonic nonlinearity to irradiated, annealed, and re-irradiated microstructure changes in RPV steels," J. Nucl. Mater. **448**, 26–32 (2014).

[16]K. H. Matlack, J. J. Wall, J.-Y. Kim, J. Qu, L. J. Jacobs, and W.-W. Viehrig, "Evaluation of radiation damage using nonlinear ultrasound," J. Appl. Phys. **111**, 054911 (2012).

[17]J. H. Cantrell, "Ultrasonic harmonic generation from fatigue-induced dislocation substructures in planar slip metals and assessment of remaining fatigue life," J. Appl. Phys. **106**, 093516 (2009).

[18]S. Plimpton, "Fast parallel algorithms for short-range molecular dynamics," J. Comput. Phys. **117**, 1 (1995).

[19]R. C. Pasianot and L. Malerba, "Interatomic potentials consistent with thermodynamics: The Fe-Cu system," J. Nucl. Mater. **360**, 118–127 (2007).

[20]M. I. Mendelev, S. Han, D. J. Srolovitz, G. J. Ackland, D. Y. Sun, and M. Asta, "Development of new interatomic potentials appropriate for crystalline and liquid iron," Philos. Mag. **83**, 3977–3994 (2003).

[21]Y. Mishin, M. J. Mehl, D. A. Papaconstantopoulos, A. F. Voter, and J. D. Kress, "Structural stability and lattice defects in copper: Ab initio, tight-binding, and embedded-atom calculations," Phys. Rev. B **63**, 224106 (2001).

[22]R. Monzen, M. L. Jenkins, and A. P. Sutton, "The bcc-to-9r martensitic transformation of Cu precipitates and the relaxation process of elastic strains in an Fe-Cu alloy," Philos. Mag. A **80**, 711–723 (2000).

[23]S. Y. Hu, Y. L. Li, and K. Watanabe, "Calculation of internal stresses around cu precipitates in the bcc Fe matrix by atomic simulation," Modell. Simul. Mater. Sci. Eng. **7**, 641 (1999).